Journal of the Korean Physical Society, Vol. 74, No. 7, April 2019, pp. 684∼694

Effect of Cr^{3+} Substitution on the Structural, Electrical and Magnetic Properties of $Ni_{0.7}Zn_{0.2}Cu_{0.1}Fe_{2-x}Cr_xO_4$ Ferrites

G. Satyanarayana
Advanced Analytical Laboratory, Andhra University, Visakhapatnam-530 003, India and
School of Chemistry, AU College of Science & Technology,
Andhra University, Visakhapatnam-530 003, India

G. Nageswara Rao*
School of Chemistry, AU College of Science & Technology,
Andhra University, Visakhapatnam-530 003, India

K. Vijaya Babu,† G. V. Santosh Kumar and G. Dinesh Reddy
Advanced Analytical Laboratory, Andhra University, Visakhapatnam-530 003, India

(Received 8 October 2018, in final form 3 December 2018)

In this work, $Ni_{0.7}Zn_{0.2}Cu_{0.1}Fe_{2-x}Cr_xO_4$ (x = 0.02, 0.04, 0.06, 0.08 and 0.1) ferrites were synthesized by using the solid state reaction method and how relevant properties of the samples were modified accordingly. The structural, morphological, magnetic and electrical features of the ferrites were evaluated by using X-ray diffraction, scanning electron microscopy, Fourier transmission infrared (FTIR) spectra, vibrating sample magnetometry, electron spin resonance and network analyser. The lattice constant decreases with increasing chromium concentration and the decrease in the lattice constant is attributed to the ionic radius of chromium being smaller than that of iron. The distribution of metal cations in the spinel structure was estimated from the X-ray diffraction data and showed that along with Ni^{2+} ions, most of the Zn^{2+} and the Cu^{2+} ions additionally occupied the octahedral [B] sites. The FTIR spectra revealed two prominent frequency bands in the wave number range 400–600 cm^{-1} which confirm the cubic spinel structure. The magnetic properties, such as the initial permeability, saturation magnetization and coercivity, were investigated at room temperature. The frequency-dependent dielectric constant was observed to decrease with increasing chromium concentration. This behavior was using Koops phenomenological theory.

PACS numbers: 75.50.Vv, 73.63.Bd, 61.05.cp, 75.75.–c, 77.22.–d
Keywords: Ni-Zn-Cu ferrite, Cation distribution, XRD, Magnetic properties, ESR
DOI: 10.3938/jkps.74.684

I. INTRODUCTION

Group of magnetic materials consists of ferrites, where ferrite is a general term utilized for any ferrimagnetic ceramic material. Due to the intrinsic atomic level interaction between oxygen and metal ions, ferrites have higher resistivities on the order of 10^5 to 10^7 ohm-cm compared to ferromagnetic metals [1–5]. This allows ferrites to be applied at higher frequencies and makes them technologically very valuable. The main component of iron oxide and metal oxides are ferrites. Among the different spinel ferrite materials, nickel ferrites are of great importance because of their excellent chemical stability, high electrical resistivity, high coercivity and moderate saturation magnetization [6–12]. They belong to an inverse structure category. The important magnetic properties originate mainly from the magnetic interaction between the cations that are present in the tetrahedral A and the octahedral B sites [13–16]. The nickel ferrite and the substituted nickel ferrite have been studied by a number of researchers due to their vast applications. The properties of nickel, zinc ferrite materials can be further modified by substituting with cations like copper ions. The substitution of copper in nickel ferrite enhances the properties of nickel ferrite which are useful in many device applications. Ni-Zn-Cu ferrites have emerged as important materials in recent years owing to their potential applications in power transformers in electronics, antenna in rods telecommunication, loading coils and microwave devices. In the present paper, we report the structural, magnetic, electric and dielectric properties of nickel-zinc-

*E-mail: gollapallinr@yahoo.com
†E-mail: vijayababu.k@gmail.com

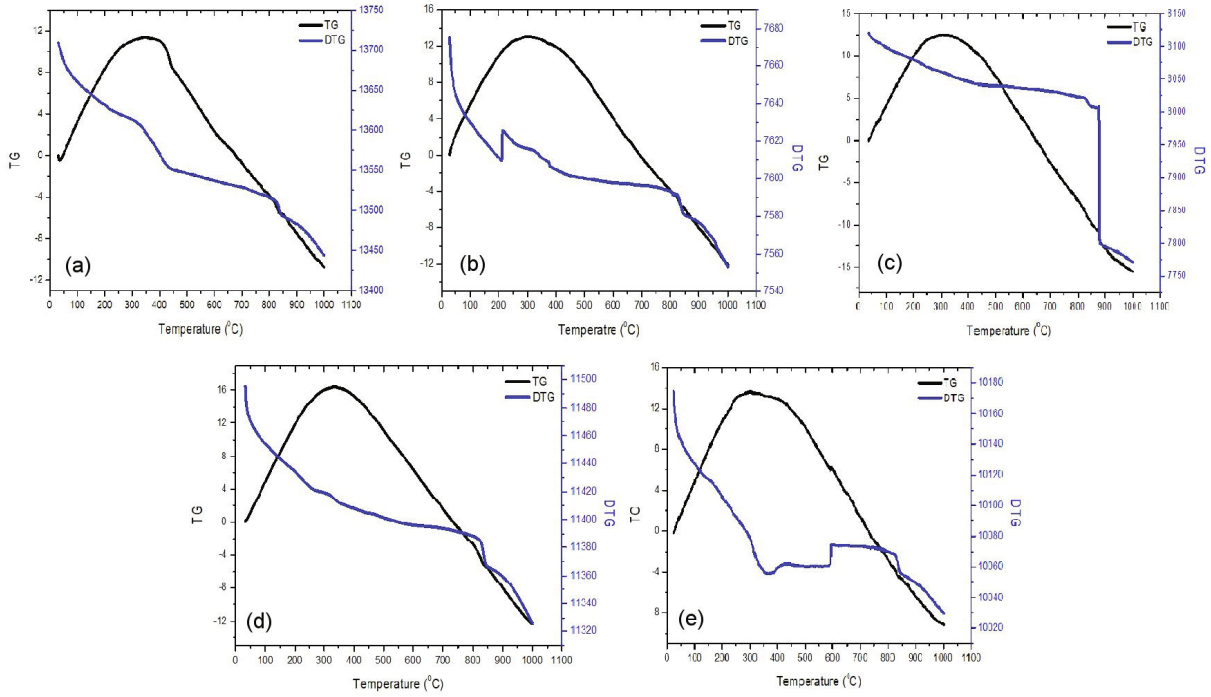

Fig. 1. (Color online) TG/DTG pattern for $Ni_{0.7}Zn_{0.2}Cu_{0.1}Fe_{2-x}Cr_xO_4$ for x = (a) 0.02, (b) 0.04, (c) 0.06, (d) 0.08, and (e) 0.1.

copper ferrite in order to study the effect of chromium at the B-site.

II. EXPERIMENTAL SET-UP

The $Ni_{0.7}Zn_{0.2}Cu_{0.1}Fe_{2-x}Cr_xO_4$ (x = 0.02, 0.04, 0.06, 0.08 and 0.1) ferrites were synthesized by the using solid state reaction method. Analytical reagent grade chemicals, such as nickel oxide (NiO), zinc oxide (ZnO), iron oxide (Fe_2O_3), copper oxide (CuO) and chromium oxide (Cr_2O_3), were used for the synthesis process. Stoichiometric proportions of these starting materials were accurately weigh and mixed thoroughly. Then the first pre-sintering of the powder was carried out at 1100°C for 5 h. The powder samples with polyvinyl alcohol (PVA) added as a binder was ground and then pressed at a force of 5 tons for 5 minutes into a circular-disk-shaped pellet. The synthesized pellet was sintered at 1200°C for 5 h and then used for further investigations of its structural, morphological, magnetic and electrical properties. The surface layers of the sintered pellet were carefully polished and washed with acetone; then, the pellet was coated with silver paste on opposite faces to act as electrodes.

The synthesized $Ni_{0.7}Zn_{0.2}Cu_{0.1}Fe_{2-x}Cr_xO_4$ (x = 0.02, 0.04, 0.06, 0.08 and 0.1) ferrites were characterized by using standard techniques such as (XRD), (SEM), (ESR) and (LCR) meter. The XRD patterns were recorded at room temperature in the 2θ range of 10° to 70° by using PANalytical, X-Pert pro with Cu-K radiation ($\lambda = 1.5405$ Å). The particle morphology of the powders was observed using SEM images taken with a JEOL JSM-6610L system. Fourier transform infrared (FT-IR) spectra measurements were accomplished using a Shimadzu IR-Prestige21 instrument and the transmittance method with potassium bromide (KBr) as the IR window in the wave- number region from 400 to 1300 cm^{-1}. The magnetic properties were measured using a JEOL-JES-FA100 ESR spectrometer with the X-band at room temperature. The impedance study was performed by using a Wayne-Kerr high- frequency LCR meter Model 65120 in the frequency range from 100 Hz to 120 MHz at room temperature. The initial permeability was determined with 10 turns of SWG enameled copper wire on a toroid and inductance measurements were carried out at various frequencies by using a Wayne-Kerr high frequency LCR meter Model 65120 in the frequency range from 100 Hz to 120 MHz at room temperature.

III. RESULTS AND DISCUSSION

1. Thermogravemetric /differential thermo gravimetric analysis

TG/DTA measurements were performed to investigate the mass loss and thermal decomposition of the synthesized $Ni_{0.7}Zn_{0.2}Cu_{0.1}Fe_{2-x}Cr_xO_4$ (x = 0.02,

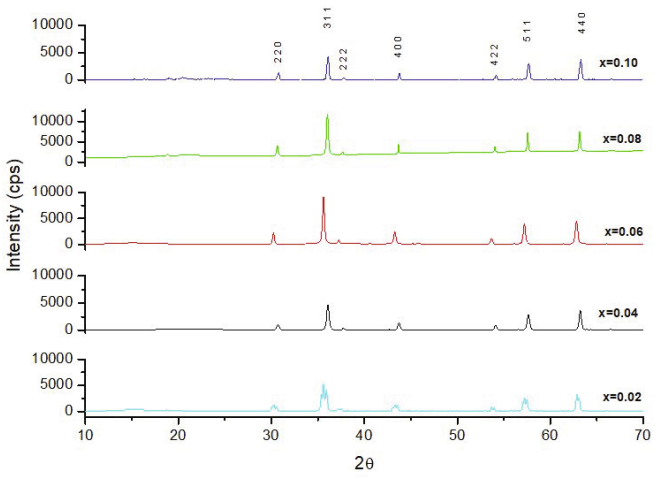

Fig. 2. (Color online) X-ray diffraction patterns for $Ni_{0.7}Zn_{0.2}Cu_{0.1}Fe_{2-x}Cr_xO_4$ (x = 0.02, 0.04, 0.06, 0.08, and 0.1).

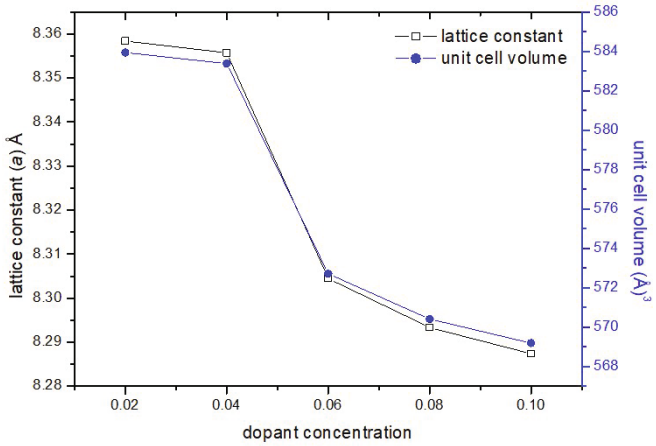

Fig. 3. (Color online) Variation of the lattice constant and unit cell volume with dopant concentration.

0.04, 0.06, 0.08 and 0.1) ferrites. Thermal analyses of the synthesized powders were carried out by using thermo gravimetric analysis (TG)/differential thermo-gravimetric analysis (DTG) and the results are shown Fig. 1. The Maxima of the exothermic peaks were observed initially at 300–400°C and were attributed to weight loss because of decomposition of organic residues and chemically bound water. The systematic faster decrease of the curve in the TG pattern suggests burn out of the organic material or the water content in the temperature range of 30–400°C, leading to crystallization process at higher temperature condition. Weight loss is minimum above temperature >400°C, confirming the conversion of oxides into a ferrite spinel phase with crystal growth. An additional exothermic peak with minimum weight loss occurs around ∼818–830°C, and it could be attributed to the formation of ferrite. Further weight loss is not observed above 830°C, leads to our assumption that the samples had to be sintered at a temperature above 850°C. With our previous studies, we maintained our current sintering temperature over 1200°C/5 hours [16–18].

Table 1. Interplaner spacing (d) for $Ni_{0.7}Zn_{0.2}Cu_{0.1}Fe_{2-x}Cr_xO_4$ (x = 0.02, 0.04, 0.06, 0.08 and 0.1) ferrites.

Plane	Interplanar distance (d) (Å)				
$h\ k\ l$	$x = 0.02$	$x = 0.04$	$x = 0.06$	$x = 0.08$	$x = 0.10$
2 2 0	2.9080	2.9538	2.9162	2.8967	2.9500
3 1 1	2.4870	2.5190	2.4925	2.4941	2.5343
2 2 2	2.3835	2.4124	2.3880	2.4467	2.4973
4 0 0	2.06853	2.0888	2.0724	2.0666	2.0883
4 2 2	1.6931	1.7061	1.6967	1.6910	1.6863
5 1 1	1.5978	1.6086	1.5996	1.5962	1.6131
4 4 0	1.4692	1.4779	1.4705	1.4716	1.4720

2. X-ray diffraction

The indexed XRD patterns for all the samples corresponding to the as-burnt powder of the $Ni_{0.7}Zn_{0.2}Cu_{0.1}Fe_{2-x}Cr_xO_4$ (x = 0.02, 0.04, 0.06, 0.08 and 0.1) ferrites are shown in Fig. 2. The patterns are indexed by different Bragg reflections, the strongest of which comes from the (311) plane, which denotes the spinel phase. The pattern clearly shows a pure cubic spinel ferrite phase with reflections due to the (220), (311), (222), (400), (422), (511) and (440). The analysis of the XRD pattern reveals the formation of single-phase compounds. No extra peaks other than cobalt ferrite are present in the XRD patterns of the prepared samples. The XRD data for the present samples were used to determine the various structural parameters. From the X-ray peak broadening of the (311) peak, the crystallite size of the synthesized ferrites were calculated using Scherrer formula. Table 2 shows that the values of the crystallite size vary in the range from 5 to 14 nm. The particle size is not the same for all compositions, even though all the samples were prepared under identical condition. The variation in the crystallite size occurred due to the preparation conditions, which give rise to different rates of ferrite formation for different concentrations of chromium.

The average value of the lattice parameter (a), calculated from various Braggs reflections observed in the XRD pattern of each samples are given in the Table 2. The lattice constant (a) varies from 8.2873 Å to 8.3584 Å. The lattice constant decreases with increasing chromium content from $x = 0.02$ to 1.0. The variation in the lattice parameter (a) shows a linear chromium content dependence, as shown in Fig. 3. The lattice constant variation depends upon the ionic radii of the dopant ions. A decrease in the lattice constant is observed for an increase in the Cr^{3+} content in the synthesised ferrite system. A

Table 2. Lattice constant, cell volume, X-ray density, strain and crystallite size for $Ni_{0.7}Zn_{0.2}Cu_{0.1}Fe_{2-x}Cr_xO_4$ (x = 0.02, 0.04, 0.06, 0.08 and 0.1) ferrites.

x-value	Lattice constant (Å)	Volume (Å)^3	X-ray density (g·cm^{-3})	Crystallite size (nm)	Molecular weight (g)
0.02	8.3584	583.9413	5.5058	5.6047	236.1286
0.04	8.3557	583.3801	5.4994	6.9642	236.0516
0.06	8.3044	572.7076	5.4737	7.3155	235.9746
0.08	8.2932	570.4018	5.3701	14.0197	235.8977
0.10	8.2873	569.1781	5.3700	9.2875	235.8207

Table 3. Ionic radii of the tetrahedral A-site (r_A) and the octahedral B-site (r_B) and theoreticallylattice constant (a_{th}) and oxygen positional parameter (u) for $Ni_{0.7}Zn_{0.2}Cu_{0.1}Fe_{2-x}Cr_xO_4$ (x = 0.02, 0.04, 0.06, 0.08 and 0.1) ferrites.

x-value	r_A (Å)	r_B (Å)	a_{th} (Å)	u-value (Å)
0.02	0.613	0.6492	8.2293	0.3890
0.04	0.613	0.6494	8.2287	0.3890
0.06	0.613	0.6496	8.2283	0.3890
0.08	0.613	0.6498	8.2275	0.3890
0.10	0.613	0.6500	8.2272	0.3890

decrease in lattice constant is reasonably expected and can be attributed to the substitution of Cr^{3+} with a smaller ionic radii of Cr^{3+} (0.64 Å) for Fe^{3+} with a larger ionic radius (0.67 Å) in the present ferrite system. It also causes an increase in the interatomic spacing parameter d, shown in Table 1. The variation in the lattice parameter with chromium content x obeys Vegards law. The value of the lattice parameter for the present nickel ferrite sample was found to be 8.3259 Å, which is fairly closed to the reported value. A similar type of variation in the lattice constant was observed for chromium-substituted nickel ferrite [19,20].

The hopping lengths (L_A and L_B) between magnetic ions (the distance between the ions) in the tetrahedral A site and the octahedral B sites can be calculated, and the values of the hopping lengths are listed in Table 5. The variations in the hopping lengths decreased with increased chromium substitution, a behavior similar to that of the lattice constant. The result can be explained on the basis of the variation in the lattice constant with dopant concentration, Table 5 shows clearly decreases in the L_A and the L_B values.

3. Theoretical lattice constant

In order to verify the cation distribution, we calculated theoretical lattice parameters from the following relation and compared the values with experimental results,

$$a_{th} = \Big(\frac{8}{3\sqrt{3}}\Big)(r_A + r_o) + \sqrt{3}(r_B + r_o) \qquad (1)$$

where r_A is tetrahedral sites radius, r_B is the octahedral sites radius, and r_o is the radius of the oxygen ion (1.32 Å). The ionic radii of the tetrahedral (r_A) and the octahedral (r_B) sites are calculated by using the following relations:

$$\begin{aligned} r_A &= [0.1(Cu_A^{2+}) \cdot r(Cu_A^{2+}) + 0.9(Fe_A^{3+}) \cdot r(Fe_A^{3+})] \\ r_B &= [0.7(Ni_A^{2+}) \cdot r(Ni_A^{2+}) + 0.2(Zn_B^{2+}) \cdot r(Zn_B^{2+}) + x(Cr_B^{3+}) \cdot r(Cr_B^{3+}) + 2 - x(Fe_B^{3+}) \cdot r(Fe_B^{3+})]/2 \end{aligned} \qquad (2)$$

where $r_{Ni^{2+}}$, $r_{Cu^{2+}}$, $r_{Zn^{2+}}$ $r_{Cr^{3+}}$ and $r_{Fe^{3+}}$ are the cationic radii of Ni, Cu, Zn, Cr and Fe ions, respectively taken from the work of Shannon. From Table 4, clearly, the cation distribution based on X-ray intensity calculations is in close to the real distribution. The table shows that r_A is constant and r_B increases with increasing chromium concentration. The theoretical and the experimental lattice parameters have the same decreasing trends. The difference is that the theoretical lattice constants are a little higher than the experimentally determined values. This variation is due to the occupation of A sites by the chromium ions and the replacing of iron ions in B sites [21].

The oxygen parameter (u-value) is determined by using the formula

$$u = \Big[(r_A + r_o)\frac{1}{\sqrt{3a}} + \frac{1}{4}\Big] \qquad (3)$$

In the spinel structure, the oxygen positional parameter has a value in the neighbourhood of 0.375 Å for which

Table 4. Cation distribution and intensity ratios for $Ni_{0.7}Zn_{0.2}Cu_{0.1}Fe_{2-x}Cr_xO_4$ (x = 0.02, 0.04, 0.06, 0.08 and 0.1) ferrites.

x-value	Cation distribution	$I_{(220)}/I_{(400)}$		$I_{(422)}/I_{(440)}$		$I_{(220)}/I_{(440)}$	
		Obs.	Cal.	Obs.	Cal.	Obs.	Cal.
0.02	$[Cu_{0.1}Fe_{0.9}][Ni_{0.7}Zn_{0.2}Fe_{1.08}Cr_{0.02}]O_4$	0.7485	0.7478	0.2607	0.2607	0.2858	0.2837
0.04	$[Cu_{0.1}Fe_{0.9}][Ni_{0.7}Zn_{0.2}Fe_{1.06}Cr_{0.04}]O_4$	0.8952	0.8906	0.2621	0.2599	0.4845	0.4828
0.06	$[Cu_{0.1}Fe_{0.9}][Ni_{0.7}Zn_{0.2}Fe_{1.04}Cr_{0.06}]O_4$	0.8239	1.1294	0.5036	0.4664	0.4625	0.5413
0.08	$[Cu_{0.1}Fe_{0.9}][Ni_{0.7}Zn_{0.2}Fe_{1.02}Cr_{0.08}]O_4$	0.0220	0.0274	0.4159	0.5066	0.0137	0.0194
0.10	$[Cu_{0.1}Fe_{0.9}][Ni_{0.7}Zn_{0.2}Fe_{1.00}Cr_{0.1}]O_4$	0.9316	0.9706	0.3341	0.3099	0.4799	0.4814

Table 5. Hopping lengths L_A and L_B, tetrahedral bond (d_{AL}), octahedral bond (d_{BL}), tetrahedral edge (d_{AE}) and octahedral edge (d_{BE}) (shared and unshared) for $Ni_{0.7}Zn_{0.2}Cu_{0.1}Fe_{2-x}Cr_xO_4$ (x = 0.02, 0.04, 0.06, 0.08 and 0.1) ferrites.

x-value	L_A (Å)	L_B (Å)	d_{AL}	d_{BL}	d_{AE}	d_{BE}	d_{BEU}
0.02	3.6192	2.9551	2.0123	1.9795	3.2861	2.6241	2.9643
0.04	3.6181	2.9541	2.0116	1.9788	3.2850	2.6233	2.9634
0.06	3.5959	2.9360	1.9993	1.9667	3.2648	2.6072	2.9452
0.08	3.5911	2.9321	1.9966	1.9640	3.2605	2.6037	2.9413
0.10	3.5885	2.9300	1.9952	1.9626	3.2582	2.6018	2.9392

the arrangement of O^{2-} ions corrosponds exactly to cubic closed packing. However, in our case, The u-value is found to be 0.3890 Å. This value is larger than the ideal value (u = 0.375 Å); this may be due to the history of the samples or to experimental or measurement errors. It also may be attributed to the small displacements of the anions from the ideal situation to form extended tetrahedral interstices [22,23]. Using the experimental values from the oxygen positional parameter u and the lattice parameter a, we calculated the interionic distances, *i.e.*, octahedral and tetrahedral bond lengths d_{BL} and d_{AL}, tetrahedral edge, shared and unshared octahedral edge (d_{AE}, d_{BE} and d_{BEU}), and the values are listed in Table 5. Clearly the values of d_{AE}, d_{AL}, d_{BE}, d_{BL} and d_{BEU} decreasing with increase in chromium concentration. This variation may be attributed to the substitution a cation and its distribution.

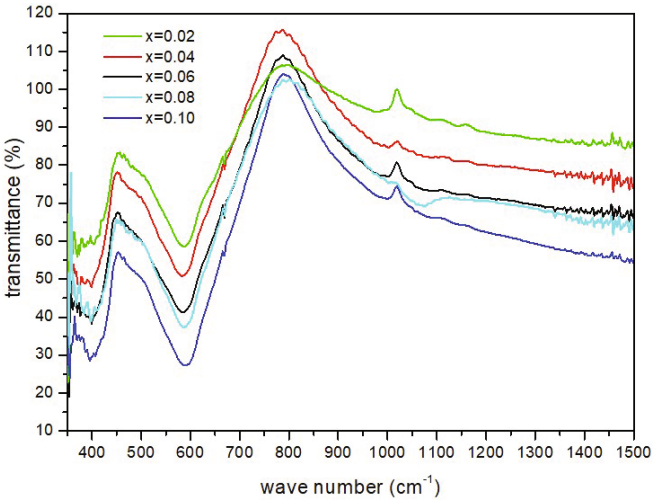

Fig. 4. (Color online) FTIR spectra of $Ni_{0.7}Zn_{0.2}Cu_{0.1}Fe_{2-x}Cr_xO_4$ (x = 0.02, 0.04, 0.06, 0.08, and 0.1)

4. Fourier-transforms infrared spectroscopy

Figure 4 describes the FTIR spectra of $Ni_{0.7}Zn_{0.2}Cu_{0.1}Fe_{2-x}Cr_xO_4$ (x = 0.02, 0.04, 0.06, 0.08 and 0.1) room temperature in the 350–1500 cm^{-1} wavenumber range. In the FTIR spectra, two persistent absorption bands corresponding to stretching vibrations of octahedral and tetrahedral complexes at around ~400 and ~600 cm^{-1} can be observed and confirms the formation of a spinel ferrite structure [24]. We observe that all samples exhibit two prominent absorption bands in the ranges ~600 cm^{-1} (ν_1) and ~400 cm^{-1} (ν_2), respectively the band at ~400 cm^{-1} (ν_2) corresponds to octahedral group complexes (Fe^{3+}-O^{2-}), and the band at ~600 cm^{-1} (ν_1) corresponds to stretching vibrations of the tetrahedral groups (Fe^{3+}-O^{2-}). Table 6 represents different values of ν_1 and ν_2, the values are seen to vary slightly due to the difference in the Fe^{3+}-O^{2-} distances for the octahedral and the tetrahedral sites. In this present study, two major frequency bands are observed, a lower frequency band (ν_2) at 400 cm^{-1} and a high frequency band (ν_1) at 600 cm^{-1}. The higher frequency band (ν_1) is nearly constant for all synthesized compounds. The low frequency band (ν_2) slightly shifts to the high frequency side and the spectral band broaden with increasing chromium concentration [25]. Due to Cr higher atomic weight and smaller ionic radius compared to iron, which affects Fe^{3+}-O^{2-} distances on B sites, the

Table 6. FTIR transmittance bands for $Ni_{0.7}Zn_{0.2}Cu_{0.1}Fe_{2-x}Cr_xO_4$ (x = 0.02, 0.04, 0.06, 0.08 and 0.1) ferrites.

x-value	ν_1	ν_2	$K_t \times 10^5$ (dyne/cm)	$K_o \times 10^5$ (dyne/cm)
0.02	667.39	419.50	1.555	1.442
0.04	669.32	418.57	1.551	1.443
0.06	667.39	419.53	1.555	1.442
0.108	668.36	418.57	1.551	1.443
0.10	667.39	418.57	1.551	1.442

broadening of the spectral band and the shift in (ν_2) to the higher frequency side is attributed to chromium ions occupying octahedral (B) sites. Therefore, a slight shift of ν_2 bands towards low frequency is expected because an increase in the sites radius reduces the fundamental frequency; therefore, the center frequency of bands should shift to lower frequency side and vice versa [26, 27].

5. Scanning Electron Microscope

The scanning electron microscope provided morphological patterns of the synthesized $Ni_{0.7}Zn_{0.2}Cu_{0.1}Fe_{2-x}Cr_xO_4$ (x = 0.02, 0.04, 0.06, 0.08 and 0.1) ferrites. Clear from SEM images of the ferrite system, the particles are almost spherical in shape, but are agglomerated to some extent due to the interaction between magnetic particles. We also observe uniformly sized grains distributed throughout the surface, which exhibits a decreasing trend with increasing chromium substitution. The particle size decreases significantly with increasing dopant concentration because the ionic radius of chromium is smaller than that of iron. The clearness of the SEM images of all our samples also reveals that no secondary phases are present. This is supported by the absence of additional peaks in the XRD patterns. The micrographs of all the samples exhibit the presence of a number of smaller grains having a large number of interfaces, which have a direct effect on the properties of these ferrites. These microstructural modifications may reflect the difference in the radii of the substituting cations [28, 29]. The average grain size calculated from the instrument was found to be in the nanometre range of 10mm. The specific surface area was calculated by using the formula

$$S = \frac{6000}{D_\rho}\ \mathrm{m^2/gm}, \tag{4}$$

where ρ is the density of the particles measured in gm/cm^3, and D is the particles diameter in mm. With increasing in dopant concentration, the surface area decreases, which indicates the nanocrystalline nature of the

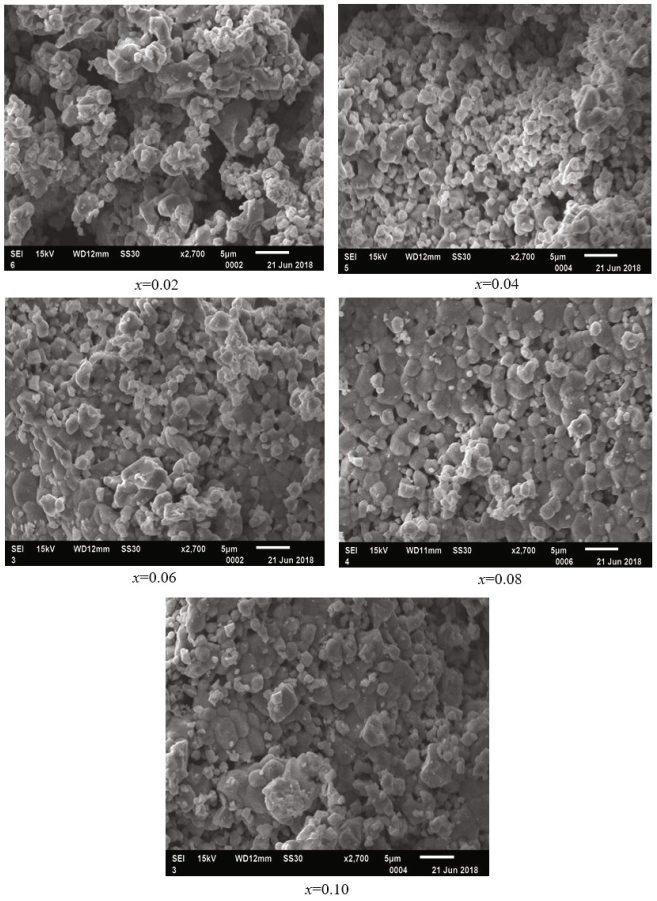

Fig. 5. SEM images of $Ni_{0.7}Zn_{0.2}Cu_{0.1}Fe_{2-x}Cr_xO_4$ (x = 0.02, 0.04, 0.06, 0.08, and 0.1).

prepared samples. The decrease in the grain size increases the surface area. As observed from the SEM images the porosity for all our samples is low. That the crystallite size and surface area play significant roles in the magnetic properties of ferrites due to the sizes of the magnetic domains; is well known.

A reliable quantitative composition analysis was done using the EDS, and measurements, the values calculated in the present system indicate that the stoichiometry of the samples were still almost the same after sintering process. The EDS spectra illustrated in Fig. 6 show the presence of the elements Ni, Zn, Cu, Cr, Fe and O without impurities. These results confirm that the final composition of the samples is the same as the starting composition without any extra impurities. The observed quantitative results indicate that the chromium concentration increases in the samples as expected based on the synthesis method. The approximate compositions estimated from the EDS data agree well with the stoichiometric chemical compositions. The compositions of chromium are found to be 0.99, 1.05, 1.30, 1.47 and 2.54, respectively.

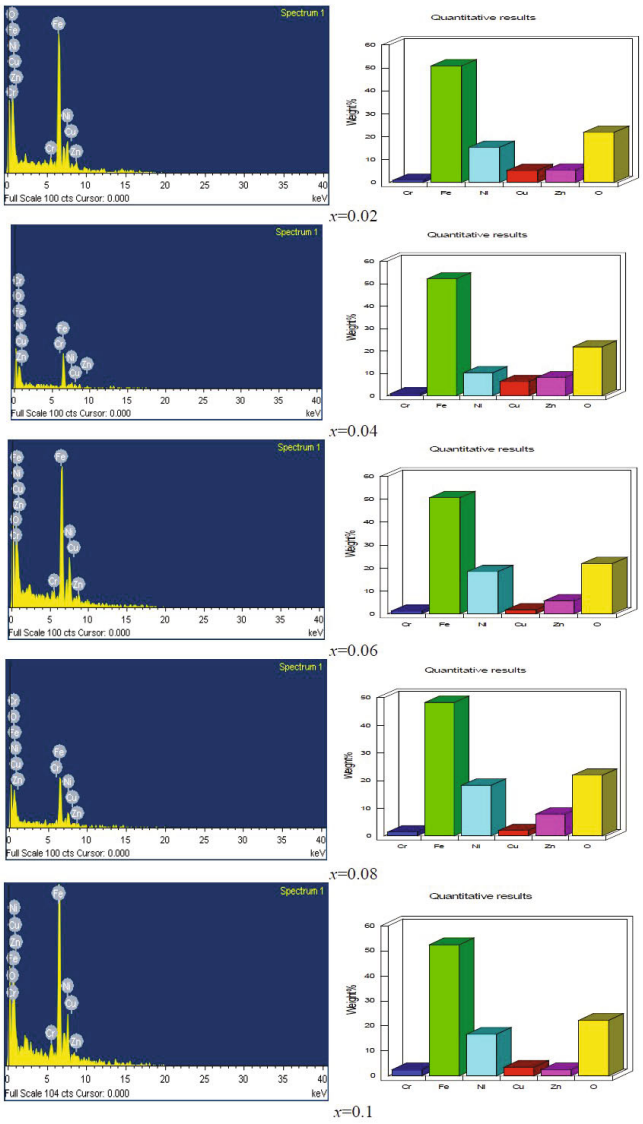

Fig. 6. (Color online) EDS images of $Ni_{0.7}Zn_{0.2}Cu_{0.1}Fe_{2-x}Cr_xO_4$ (x = 0.02, 0.04, 0.06, 0.08, and 0.1).

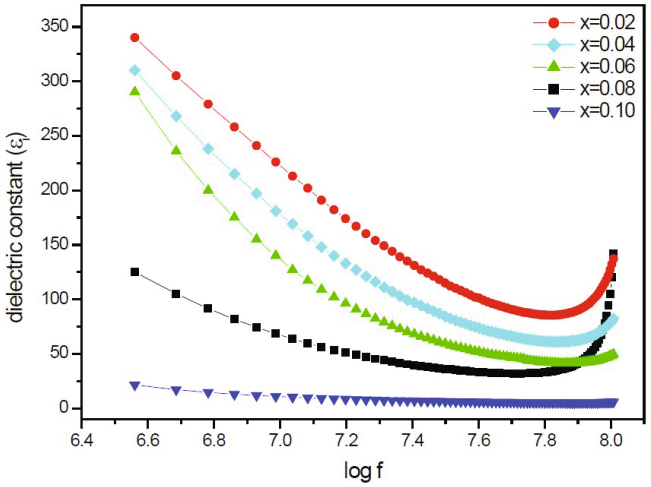

Fig. 7. (Color online) Variation of dielectric constant with frequency for $Ni_{0.7}Zn_{0.2}Cu_{0.1}Fe_{2-x}Cr_xO_4$ (x = 0.02, 0.04, 0.06, 0.08, and 0.1).

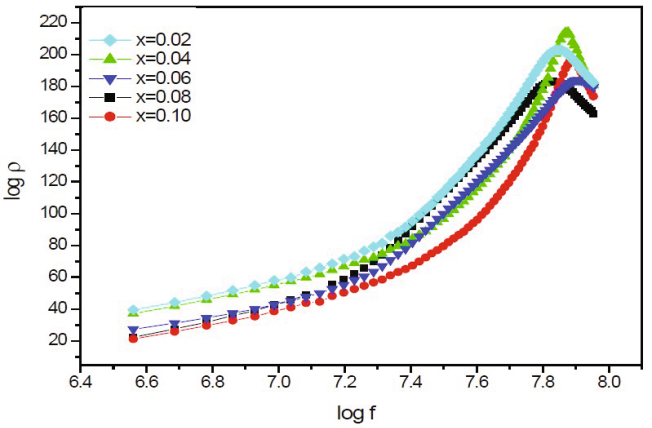

Fig. 8. (Color online) Variation of log with log frequency for $Ni_{0.7}Zn_{0.2}Cu_{0.1}Fe_{2-x}Cr_xO_4$ (x = 0.02, 0.04, 0.06, 0.08, and 0.10) ferrites.

6. Dielectric constant (ε_r)

In Fig. 7, we have presented the variation in the dielectric constant measured as a function of frequency for all synthesized ferrites under investigation at room temperature. We observe from the Fig. 6 that the dielectric constant decreases when the frequency is increase. No change in the behavior of the dielectric constant is seen for any of the different dopant concentrations, which is a normal dielectric behavior for spinel ferrites. The decrease in the dielectric constant with increasing frequency is exponential in nature and analogous to Maxwell-Wagner interfacial type polarization, which is in agreement with Koops phenomenological theory. The maximum dispersion of the dielectric constant is 0.08, which is minimum for the sample. The maximum dispersion is attributed to the fact that the number of available ferrous ions is higher than it is in other compositions. As a consequence, these ions may be polarized to the maximum possible extent. The dielectric constant decreases with the frequency of the externally applied field increases gradually (100 Hz to 120 MHz). This is because of the fact that beyond a certain frequency of the externally applied electric field, the electronic exchange between ferrous and ferric ions cannot follow the alternating field. $Fe^{2+} \leftrightarrow Fe^{3+}$ The other fact is that the electron exchange between Fe^{2+} and Fe^{3+} in n-type semiconducting ferrites and the whole exchange between Ni^{3+} and Ni^{2+} ions in p-type semiconductor ferrites cannot follow the frequency of the applied alternating field beyond a critical value of the frequency [30–33].

Table 7. g-value, resonance field, saturation magnetization (M_s), magnetic moment and coercivity (H_c) for $Ni_{0.7}Zn_{0.2}Cu_{0.1}Fe_{2-x}Cr_xO_4$ (x = 0.02, 0.04, 0.06, 0.08 and 0.10) ferrites.

x-value	g-value	Resonance field (mT)	Saturation magnetization) (M_s) (emu/gm	Magnetic moment (η_B)	Coercivity (H_c) (Oe)
0.02	1.8792	359.369	98.28375	4.149	21
0.04	1.6549	408.075	92.19975	3.987	26
0.06	1.8370	367.616	90.38775	3.821	31
0.08	2.0818	324.441	88.77375	3.752	38
0.10	1.9277	350.336	86.05575	3.635	46

7. DC resistivity (ρ)

Figure 8 shows the variation in the DC resistivity with frequency for the synthesized ferrites. With increasing frequency, the resistivity is found to also increase. For ferrites, electron hopping between Fe^{2+} and Fe^{3+} and hole hopping between Ni^{3+} to Ni^{2+} in B sites. Is well brown to occur due to the fact that the ionic radius of Cr^{3+} (0.64 Å) ions is smaller than that of Fe^{3+} (0.67 Å) ions in the present ferrite system and when the chromium is substituting for iron, some chromium or iron will occupy the tetrahedral sites, displacing those in octahedral sites, leading to a decrease in the resistivity. This increase in the Fe^{3+} or Cr^{3+} ions in octahedral sites will increase the number of Fe^{2+}, Fe^{3+} or Cr^{2+}, Cr^{3+} pairs in octahedral sites, which increases the conductivity of ferrites. Therefore, the resistivity is decreased by the addition of chromium. The decrease in the resistivity might also be related to the decrease in the porosity because the pores are non-conductive, which increases the resistivity of the material. The resistivity decreases with increasing porosity because on the charge carriers move, they encounter pores [34].

8. Magnetic properties

The magnetic properties play an important role in the applications of soft magnetic materials. The magnetic properties of the synthesized ferrite samples of $Ni_{0.7}Zn_{0.2}Cu_{0.1}Fe_{2-x}Cr_xO_4$ (x = 0.02, 0.04, 0.06, 0.08 and 0.10) were studied by using the hysteresis loops at room temperature. The variation in the saturation magnetization with applied field is shown in Fig. 9 for all compositions. The saturation magnetization decreases with increasing Cr concentration due to the Cr^{3+} cations occupying in B sites having less magnetic moment than the Fe^{3+} and to the Cr^{3+} co moving an equal number of Fe^{3+} from B to A sites. In $Ni_{0.7}Zn_{0.2}Cu_{0.1}Fe_{2-x}Cr_xO_4$ (x = 0.02, 0.04, 0.06, 0.08 and 0.10) ferrites, Ni^{2+} ions occupy octahedral (B) sites, and equal numbers of Fe^{3+} ions occupy tetrahedral (A) and octahedral sites [35,36]. This substitution decreases the number of active linkages and weakens the AB exchange interaction. This

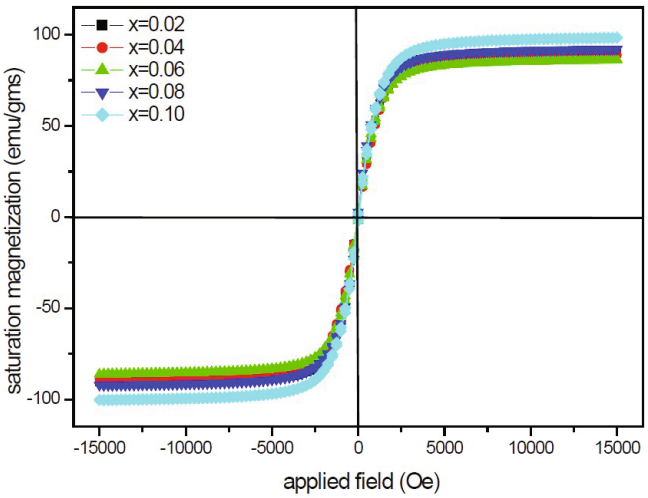

Fig. 9. (Color online) Hysteresis loops for $Ni_{0.7}Zn_{0.2}Cu_{0.1}Fe_{2-x}Cr_xO_4$ (x = 0.02, 0.04, 0.06, 0.08, and 0.10) ferrites.

exchange interaction is not sufficient to align all the iron ions at B sites in one direction, resulting in spin canting of iron ions [37]. Therefore, the magnetic moment in the A sub lattice increases while it decreases in the B sublattice, and as a result, the net magnetic moment decreases. The observed variation in the saturation magnetization can be explained on the basis of Neels theory.

According to Neels theory, the net magnetic moment is given by $n_B = M_B - M_A$, where M_B is the magnetic moment of the B-sublattice and M_A is the magnetic moment of the A sublattice.

The magnetic moments of Ni, Zn, Cu, Fe and Cr are 2 μB, 0 μB, 1 μB, 5 μB and 3 μB, respective and Neels magneton number can be obtained by using

$$n_B = \frac{\text{Molecular Weight} \times M_s}{5585} \tag{5}$$

where n_B is the magneton number of the samples, and M_s is the saturation magnetization of the samples.

The saturation magnetization gradually decreases in the system with increasing Cr content. This is due to the fact that the magnetization of a spinel cubic structure depends on the types of cations in the tetrahedral A and the octahedral B sites. When the Cr content is in-

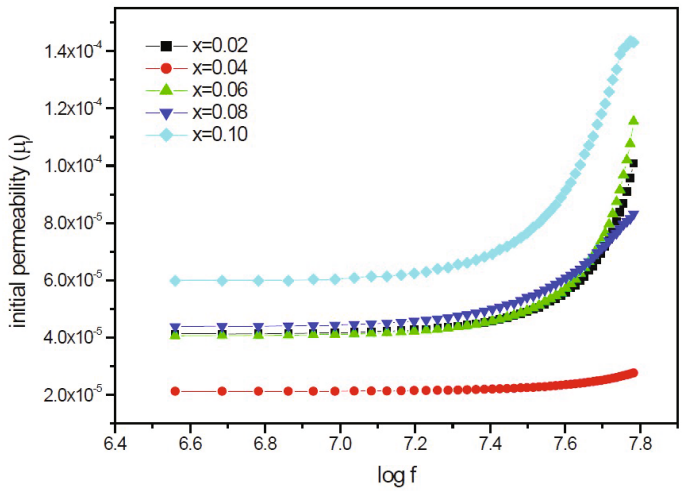

Fig. 10. (Color online) variation of the initial permeability with log frequency for $Ni_{0.7}Zn_{0.2}Cu_{0.1}Fe_{2-x}Cr_xO_4$ ($x = 0.02$, 0.04, 0.06, 0.08, and 0.10).

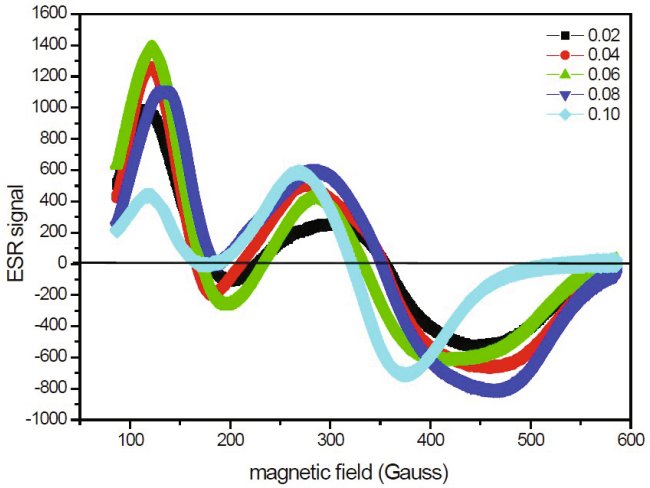

Fig. 11. (Color online) ESR spectra for $Ni_{0.7}Zn_{0.2}Cu_{0.1}Fe_{2-x}Cr_xO_4$ ($x = 0.02$, 0.04, 0.06, 0.08, and 0.10).

creased, the paramagnetic Cr^{3+} has a stronger tendency to occupy octahedral B sites. This will reduce the quantity of magnetic ions in the B sites, thereby reducing the magnetic moment of B sites, From Table 7, the coercivity increases with increasing Cr concentration. As the porosity increases with increasing Cr concentration, the coercivity is also expected to increase. With increasing porosity, a higher field is needed to push the domain wall, which results in a high coercivity [38–40].

9. Initial permeability (μ_i)

The compositional variation of the initial permeability was measured using a Waynn-Kerr network analyser at room temperature for frequencies from 20 Hz to 120 MHZ. The initial permeability of toroids can be calculated by using the formula

$$\mu_i = \frac{L}{0.0046N^2h\log\dfrac{d_2}{d_1}} \tag{6}$$

where L is the inductance in μH, N is the number of turns, d_1 is the inner diameter in cm, d_2 is the outer diameter in cm, and h is the height of the core in cm. The variations of the initial permeabilitys for all the synthesized ferrites are shown in Fig. 10. From the figure, we observe that the permeability slightly increases with increasing Cr concentration. The increased permeability is due to the combined effect of increased grain size and increased densification. Low frequency dispersion, which may be attributed to domain wall movement, is also seen. This can be attributed to the increase in grain size with increasing concentration. Increasing concentration may causes decreasing magnetic anisotropy, thereby reducing the internal stresses and crystal anisotropy, which may resulting minimum hindrance required for moving the domain walls. Thus, the initial permeability increasing with increase in dopant concentration [41–46].

10. Electron spins resonance spectroscopy

The ESR spectra of the as synthesized ferrite materials are shown in Fig. 11. The spectra of these samples show a single broad signal with a g-value of approximately 2.0, indicating the presence of Fe^{3+}, Cu^{2+}, Zn^{2+}, Cr^{3+} and Ni^{2+} ions with dominance of Fe^{3+} ions. signal. The variation in ESR parameters, such as the peak-to-peak linewidth (ΔH_{PP}), the g-value and the spin concentration of paramagnetic centers present in these ferrites, can be discussed in terms of the interparticle magnetic dipole-dipole interactions and super-exchange interactions. The interparticle super-exchange interactions between magnetic ions (through oxygen) can reduce the value of peak-to-peak linewidth. The magnitude of this interaction is determined by the relative positions of the metallic and the oxygen ions. The g-value increases with increasing chromium ion concentration in these ferrite samples due to a strengthening of the super-exchange interaction via magnetic ordering within each sublattice of ferrite through a rearrangement of cations between A and B-sites. The value of the resonance field decreases with increasing chromium content in these ferrite analogues, with an increase in intensity. The decrease in linewidth, *i.e.*, the narrowing of resonance derivative signal with respect to the increase in the chromium concentration has been attributed to chromium ions occupying octahedral B sites. The presence of Cr^{3+} ions in the octahedral B sites causes a decrease in the magnetic moment of the B sublattice. This causes an overall decrease in the total

magnetic moment. This decrease in the magnetic moment of the sample may be the reason for the decrease in the linewidth of the sample [47,48].

IV. CONCLUSION

The $Ni_{0.7}Zn_{0.2}Cu_{0.1}Fe_{2-x}Cr_xO_4$ ($x = 0.02$, 0.04, 0.06, 0.08 and 0.10) ferrites were successfully synthesized through a solid state reaction method at temperature 1100°C. The synthesized ferrites exhibited good crystal structure, fine grain size and improved initial permeability. The percentages of weight loss and gain were obtained at different temperatures by employing the thermal properties of the synthesized ferrites. X-ray diffraction confirmed the formation of a single ferrite phase with no impurities. The SEM analysis indicated uniform grain growth and less agglomeration. The FTIR spectrum exhibited two major absorption bands, one near 600 cm^{-1} and the other near 400 cm^{-1}, which are characteristic features of spinel ferrites. The initial permeability and dielectric constant was found to increase at high frequency. The dielectric study showed normal dielectric behavior for all samples and a strong influence of frequency. The saturation magnetization (M_s), which is decreased this is due to the fact that the magnetization of the spinel cubic structure depends on the types of cations in the tetrahedral A and the octahedral B sites, and the coercivity (H_c) increased as the chromium concentration was increased. The present study, thus, reveals that the solid-state- reaction method is one of the simplest effective chemical routes for preparing a wide range of ferrites for diverse applications.

ACKNOWLEDGMENTS

The authors are grateful to Department of Science and Technology (DST), Government of India, New Delhi, for providing financial support through (DST)-Promotion of University Research and Scientific Excellence (PURSE) Programme.

REFERENCES

[1] E. Schloemann, J. Magn. Magn. Mater. **209**, 15 (2000).
[2] S. Sharma, K. Verma, U. Chaubey, V. Singh and B. R. Mehta, Mater. Sci. Eng. B **167**, 187 (2010).
[3] D. R. Patil and B. K. Chougule, Mater. Chem. Phys. **117**, 35 (2009).
[4] R. V. Mangalaraja, S. A. Kumar, P. Manohar and F. D. Gnanam, J. Magn. Magn. Mater. **253**, 56 (2002).
[5] L-Z. Li, X-X. Zhong, R. Wang and X-Q. Tu, J. Magn. Magn. Mater. **435**, 58 (2017).
[6] F. Li, J. J. Liu, D. G. Evans and X. Duan, Chem. Mater. **16**, 1597 (2004).
[7] A. V. Knyazev *et al.*., J. Magn. Magn. Mater. **435**, 9 (2017).
[8] S. T. Alone, S. E. Shirsath, R. H. Kadam and K. M. Jadhav, J. Alloys Compd. **509**, 5055 (2011).
[9] N. Rezlescu, L. Rezlescu, P. D. Popa and E. Rezlescu, J. Magn. Magn. Mater. **215-216**, 194 (2000).
[10] S. Dey *et al.*, J. Appl. Phys. **114**, 093901 (2013).
[11] JH. Jean, CH. Lee and WS. Kou, J. Am. Ceram. Soc. **82**, 343 (1999).
[12] W. A. Bayoumy and M. A. Gabal, J. Alloys Compd. **506**, 205 (2010).
[13] A. I. Borhan, V. Hulea, A. R. Iordan and M. N. Palamaru, Polyhedron **70**, 110 (2014).
[14] H. Su, H. Zhang, X. Tang, Z. Zhong and Y. Jing, Mater. Sci. Eng. B **162**, 22 (2009).
[15] W-C. Hsu, S. C. Chen, P. C. Kuo, C. T. Lie and W. S. Tsai, Mater. Sci. Eng. B **111**, 142 (2004).
[16] X-M. Liu and W-L. Gao, Mater. Manuf. Processes **27**, 905 (2012).
[17] P. P.Hankare, K. R.Sanadi, K. M.Garadkar, D. R. Patil and I. S. Mulla, J. Alloys Compd. **553**, 383 (2013).
[18] S. Singhal, S. Jauhar, J. Singh, K. Chandra and S. Bansal, J. Mol. Struct. **1012**, 182 (2012).
[19] A. R. Das, V. S. Ananthan and D. C. Khan, J. Appl. Phys. **57**, 4189 (1985).
[20] M. Hashim *et al.*, J. Alloys Compd. **549**, 348 (2013).
[21] M. Hashim *et al.*, Ceram. Int. **39**, 1807 (2013).
[22] M. Y. Lodhi *et al.* Curr. Appl. Phys. **14**, 716 (2014).
[23] P. B. Belavi, G. N. Chavan, L. R. Naik, R. Somashekar and R. K. Kotnala, Mater. Chem. Phys. **132**, 138 (2012).
[24] R. D. Waldron, Phys. Rev. **9**, 1727 (1955).
[25] R. Ali *et al.*, J. Alloys Compd. **584**, 363 (2014).
[26] P. Priyadharsini, A. Pradeep, P. S. Rao and G. Chandrasekaran, Mater. Chem. Phys. **116**, 207 (2009).
[27] S. Singhal and K.Chandra, J. Solid State Chem. **180**, 296 (2007).
[28] M. N. Akhtar *et al.*, J. Magn. Magn. Mater. **421**, 260 (2017).
[29] X. Wu, W. Wu, L. Qin, K.Wang and S. Ou *et al*, J. Magn. Magn. Mater. **379**, 232 (2015).
[30] C. G. Koops, Phys. Rev. **83**, 121 (1951).
[31] N. Rezlescu and E. Rezlescu, Phys. Status Solidi A **23**, 575 (1974).
[32] A. S. Fawzi, A. D. Sheikh and V. L. Mathe, J. Alloys Compd. **502**, 231 (2010).
[33] R. Peelamedu, C. Grimes, D. Agrawal, R. Roy and P. Yadoji, J. Mater. Res. **18**, 2292 (2003).
[34] T. J. Shinde, A. B. Gadkari and P. N. Vasambekar, Mater. Chem. Phys. **111**, 87 (2008).
[35] K. Huang *et al.*, High Temp. Mater. Proc. **35**, 531 (2016).
[36] L. L. Lang *et al.*, J. Appl. Phys. **116**, 123901 (2014).
[37] A. K. Singh, T. C. Goel and R. G. Mendiratta, J. Magn. Magn. Mater. **281**, 276 (2004).
[38] K. Sun *et al.*, J. Magn. Magn. Mater. **320**, 3352 (2008).
[39] W. Zhang, X. Zuo, D. Zhang, C. Wu and S. R. P. Silva, Nano Tech. **27**, 245707 (2016).
[40] R. H. Kadam, A. Karim, A. B. Kadam, A. S. Gaikwad and S. E. Shirsath, Int. Nano Lett. **2**, 28 (2012).
[41] P. S. Aghav *et al.*, Physica B: Condens. Matter **406**, 4350

(2011).
[42] Z. H. Khan, M. M. Rehman, S. S. Sikder, M. A. Hakim and D. K. Saha, J. Alloys Compd. **548**, 208 (2013).
[43] J. S. Ghodaken, T. J. Shinde, R. P. Patil, S. B. Patil and S. S. Suryavanshi, J. Magn. Magn. Mater. **378**, 436 (2015).
[44] A. P. Guimaraes and I. S. Oliveira, *Magnetism and Magnetic Resonance in Solids* (John Wiley & Sons, New Jersey, 1998), p. 298.
[45] K. O. Low and F. R. Sale, J. Magn. Magn. Mater. **246**, 30 (2002).
[46] M. Kaiser, J. Phys. Chem. Solids **71**, 1451 (2010).
[47] S. A. V. Prasad *et al.*, Ceram. Int. **44**, 10517 (2018).
[48] K. V. Babu, B. Sailaja, K. Jalaiah, P. T. Shibeshi and M. Ravi, Physica B: Condens. Matter **534**, 83 (2018).